Dynamics of a non-rigid orbital siphon at a near-Earth asteroid*

Andrea Viale †, Colin McInnes ‡ and Matteo Ceriotti §
University of Glasgow, Glasgow, Scotland G12 8QQ, United Kingdom

The orbital siphon is a novel concept for propellantless payload transfer from the surface of a rotating body to orbit. In the context of asteroid mining, the orbital siphon represents an efficient solution to deliver mined material from the asteroid surface to an orbiting station for later processing or storage. The key idea is that the centrifugal-induced force exerted on a tether-connected chain of payload masses assembled from the surface of a rotating body can be large enough to pull the lower masses, to initialize an orbital siphon effect: new payloads are connected to the chain while upper payloads are removed. In this paper, the dynamics of an orbital siphon anchored to two irregularly shaped near-Earth asteroids is investigated. The siphon is modelled as a closed chain of tether-connected buckets, kept taut by two pulleys, one at the asteroid surface and one attached to an orbiting collecting spacecraft. Buckets are filled with asteroid material, to be delivered to the collecting spacecraft. It is shown that the irregularities of the gravitational field do not introduce instabilities to the orbital siphon system for the scenarios presented in this paper. Without any braking mechanism required, the average speed of the siphon does not diverge but reaches a constant value at a steady-state. Moreover, it is shown that the siphon effect is still generated when the anchor moves on the asteroid surface, allowing the mining location to be moved without interrupting the flow of material to the collecting spacecraft.

Nomenclature

E = tether axial Young Modulus

A = tether cross section

l = tether unstrained length

L = Siphon length

k, c = contact stiffness and damping on the first payload of the lifting side

*Presented at 2019 Astrodynamics Specialist Conference, Portland, ME. Paper 19-708

†Ph.D. Candidate. Division of Systems, Power and Energy. James Watt School of Engineering; a.viale.1@research.gla.ac.uk

‡James Watt Chair, Professor of Engineering Science. Division of Systems, Power and Energy. James Watt School of Engineering; colin.mcinnes@glasgow.ac.uk

§Lecturer in Space Systems Engineering. Division of System, Power and Energy. James Watt School of Engineering; matteo.ceriotti@glasgow.ac.uk

m_{cs} = collecting spacecraft mass

m_p = payload mass

m_b = bucket mass

n = number of buckets

ω = asteroid angular velocity

$\mathbf{r}_i$ = position vector of the i-th bucket of the siphon

U = asteroid gravitational potential

V = asteroid effective potential

ρ = asteroid density

G = gravitational constant

$\mathbf{F}^i_{tether}$ = forces by tethers connected to i-th bucket

$\mathbf{F}^{cs}_{tether}$ = forces by tethers connected to collecting spacecraft

$\mathbf{F}^{p1}$ = contact forces acting on the first payload on the lifting side

ϵ_i = i-th tether strain

$\mathbf{q}_i$ = relative displacement between i-th and $(i+1)$-th bucket

I. Introduction

Exploitation of space resources is one of the key challenges for the future of space exploration. Earth-based observations, as well as recent robotic missions, have shown that near-Earth asteroids could provide a range of useful resources, in some cases more accessible than lunar material [1]. Among the available resources are metals (in particular platinum-group metals) and volatiles - such as water. The latter, in particular, would provide consumables and propellant for in-orbit manufacturing, thus revolutionizing space transportation and solar system exploration [2].

A range of studies have been devoted to the analysis of asteroid mining scenarios. However, the problem of gathering material from the surface for later processing is still largely unexplored. Some authors envision the direct launch of material from the asteroid surface into orbit or for material sorting [3, 4]. However, this requires external work to be done in launching the asteroid material. Moreover, this scenario is affected by uncertainties when launching material from the surface, for example for repeatability of mass driver launches. Uncertainties in the initial condition at launch might challenge in-orbit collection of material within the micro-gravity environment at asteroids, possibly requiring large structures for material collection.

In this paper, a propellantless self-sustaining structure to deliver material from the asteroid surface to an orbiting collecting spacecraft (CS) is considered. The structure physically connects a point on the asteroid surface to the CS, thus avoiding any targeting issues. At the core of the concept, the so-called *orbital siphon* (originally devised by Davis [5, 6]),

is a chain of tethered-connected payloads, long enough such that the overall centripetal pull due to the asteroid rotation overcomes the gravitational force acting on each payload. This allows the entire chain to lift payloads: such an *orbital siphon effect* can be exploited to deliver a continuous mass flow of material from the surface of the asteroid the CS.

Use of tethered systems for asteroid missions has been widely explored in literature for different applications such as asteroid deflection [7, 8], tether-assisted asteroid observation [9] or asteroid artificial spinning [10] and de-spinning [11]. The orbital siphon, however, is a direct evolution of the space elevator [12, 13] concept where, rather than a single payload ascending along the tether a chain of tether-connected payloads is envisaged.

The authors have previously studied the dynamics of the siphon under different sets of assumptions and approximations. In Reference [14] the siphon dynamics is studied assuming that the chain of masses can slide on a rigid support anchored to the equator of a spherical asteroid. This avoids any rotation of the chain generated by inertial forces. Under these simplifying hypotheses the dynamics can be studied analytically. In particular, it was shown that the asteroid mass reduction lowers the siphon effect over time, until the siphon can no longer lift material after a certain fraction of asteroid mass has been removed. It has been shown that, for a siphon with constant length and an asteroid initially rotating at its critical angular velocity (i.e., at a spin rate at which the centrifugal-induced force on a particle at the asteroid equator equals in magnitude the gravitational force) about 8% of the initial asteroid mass can be disassembled using a constant-length siphon.

In Reference [15] it was proposed that the payload masses could slide on a tether acting as a support structure, similar to the space elevator concept but with multiple tether-connected payloads instead of a single payload. The chain of payloads would then lift thanks to the orbital siphon effect. A ballast mass at the top of the support tether can be used to reduce the equatorial oscillations of the system, induced by the inertial Coriolis forces.

In this paper, the hypothesis of a rigid structure supporting the sliding payload masses is removed and the siphon is modeled as a n-body closed chain of buckets, kept in tension by two pulleys, one at the surface of the asteroid and one attached to an orbiting collecting spacecraft (CS). Buckets are filled with asteroid material, which will be termed the *payload*. When a bucket reaches the upper pulley at the CS, the payload is released to the CS while the bucket will then descend towards the anchor pulley. Similar to a bucket-conveyor, the chain of buckets continuously cycles, due to the siphon effect generated on the lifting side of the chain. Moreover, the gravitational environment of the asteroid is simulated using three dimensional triangular-faced polyhedron shape models of near-Earth asteroids 101955 Bennu and 6489 Golevka.

The paper is structured as follows. The dynamical system, the asteroid gravitational potential and assumptions are firstly introduced. Then, results under different scenarios are presented, by varying siphon parameters and the asteroid properties. Siphons with a moving base are also analyzed. Practical aspects related to the siphon deployment and operation are examined. Finally, the effects of the solar gravitational perturbation and solar radiation pressure are discussed.

II. System description, assumptions and dynamical model

The key idea behind the orbital siphon concept is that a chain of tethered connected payload masses arranged from the surface of a rotating asteroid experiences a net radial force which can be exploited to raise the entire chain without any external force. In the scenario presented in this paper the chain of masses is designed similar to a bucket conveyor (see Fig. 1), with consecutive buckets connected to neighboring buckets via massless elastic tethers with axial Young modulus E, constant cross section A, viscosity coefficient C and unstrained length l. The siphon length L is here defined as half the unstrained length of the chain loop, i.e., $L = nl/2$. Buckets on the *lifting side* (LS) are filled with payload masses m_p, i.e., raw material mined from the asteroid. The *descending side* (DS) of the siphon hosts empty buckets, returning to the asteroid surface for refilling, after having released their payload mass to the CS, which is physically connected to the siphon through a pulley. Another pulley at the anchor ensures continuous cycling of the buckets. It is

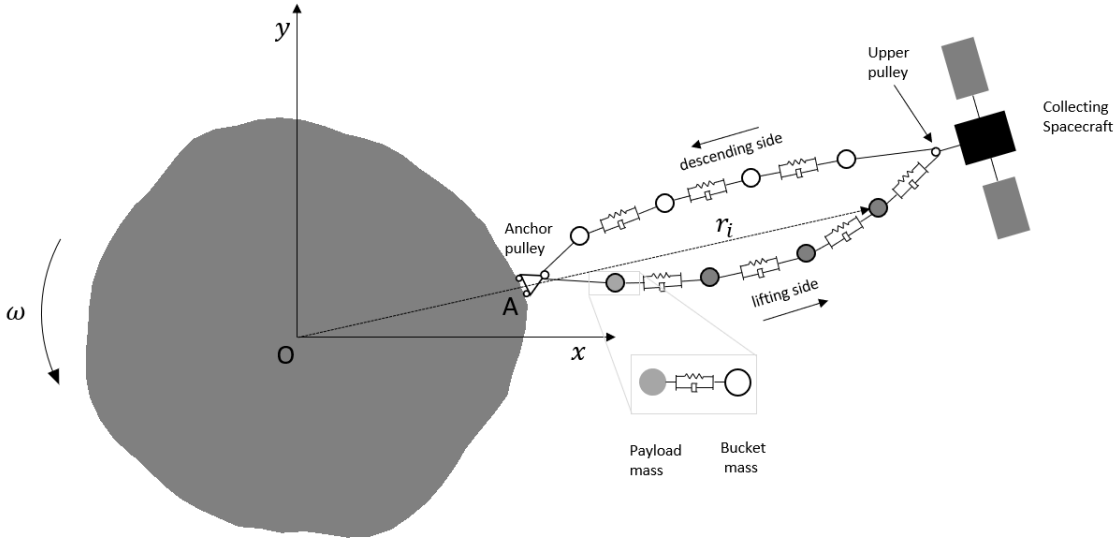

Fig. 1 Dynamical model of an orbital siphon anchored to a rotating asteroid. For clarity the siphon is represented on the asteroid $x - y$ plane.

assumed that the pulley size is much smaller than L and therefore the pulleys are modeled as point masses. This choice offers significant savings in computational time with respect to a finite-size pulley. In fact, a finite-size pulley would require modeling of the tether with intermediate nodes, separated by a distance smaller then the diameter of the pulley itself, thus considerably increasing the number of degrees of freedom of the system. Any friction between the tether and the pulley is neglected.

When a bucket reaches the anchor pulley, it is refilled with a new payload. In References [14, 15] this event was modeled as an inelastic impact, resulting in a discontinuous velocity change of the system (note that the "waiting" payload is at rest with respect to the siphon, in the asteroid reference frame). This choice may cause numerical instabilities in this model. Hence, the bucket refilling is modeled using a spring-dashpot connection between the bucket and the new

payload. Then, the first bucket mass on the LS and the corresponding payload mass are considered as separate point masses, with position vectors $\mathbf{r}_1$ and $\mathbf{r}_{p1}$ respectively, connected via a spring with stiffness k and damping constant c. Once the bucket reaches a sufficient altitude, the payload is then fixed to the bucket. Here, it is chosen to fix the payload to the bucket when another bucket reaches the anchor. For all the other buckets on the LS, the mass of the payloads is simply summed to that of the bucket, without considering two separate masses.

It is assumed that the size of the CS is small with respect to the distance between the anchor and the CS center-of-mass. For this reason, the CS is also modeled as a point mass, located in the same position as the upper pulley. Although this choice does not allow a model of the CS attitude, this approximation permits the effect of the CS mass variation (increasing over time, as more payload masses are released) to be included into the siphon dynamics.

Let xyz be an asteroid-fixed reference frame centered on the asteroid center-of-mass with the x, y and z axes corresponding to the principal axis of smallest, intermediate and largest inertia. Let $\mathbf{r}_i$ be the position vector from the origin to the i-th bucket of the chain. The equation of motion of the i-th bucket is then

$$\ddot{\mathbf{r}}_i + 2\boldsymbol{\omega} \times \dot{\mathbf{r}}_i + \boldsymbol{\omega} \times (\boldsymbol{\omega} \times \mathbf{r}_i) = \nabla U(\mathbf{r}_i) + \mathbf{F}^i_{tether}/m_i \tag{1}$$

where $\boldsymbol{\omega}$ is the angular velocity of the asteroid, U is the gravitational potential of the asteroid and $\mathbf{F}^i_{tether}$ is the total force generated by the two tethers connected to the i-th bucket. The term m_i is the mass of the buckets, including the payload mass if the bucket is traveling on the LS. Note that the acceleration of the asteroid center-of-mass due to the asteroid orbit is neglected in Eq. (1).

The potential U can be modified to include the centrifugal potential:

$$V(\mathbf{r}_i) = \frac{1}{2}(\boldsymbol{\omega} \times \mathbf{r}_i) \cdot (\boldsymbol{\omega} \times \mathbf{r}_i) + U(\mathbf{r}_i) \tag{2}$$

such that the equations of motion reduce to

$$\ddot{\mathbf{r}}_i + 2\boldsymbol{\omega} \times \dot{\mathbf{r}}_i = \nabla V(\mathbf{r}_i) + \mathbf{F}^i_{tether}. \tag{3}$$

By extension, the equations of motion of the entire dynamical system, including the CS and the payload mass m_{p1} attached to the bucket closest to the anchor are

$$\ddot{\mathbf{r}}_i + 2\boldsymbol{\omega} \times \dot{\mathbf{r}}_i = \nabla V(\mathbf{r}_i) + \mathbf{F}^i_{tether}/m_i \tag{4a}$$

$$\ddot{\mathbf{r}}_{cs} + 2\boldsymbol{\omega} \times \dot{\mathbf{r}}_{cs} = \nabla V(\mathbf{r}_i) + \mathbf{F}^{cs}_{tether}/m_{cs} \tag{4b}$$

$$\ddot{\mathbf{r}}_{p1} + 2\boldsymbol{\omega} \times \dot{\mathbf{r}}_{p1} = \nabla V(\mathbf{r}_{p1}) + \mathbf{F}^{p1}/m_{p1} \tag{4c}$$

where $\mathbf{r}_{cs}$ is the position vector of the CS, $\mathbf{F}^{cs}_{tether}$ represents the tether forces acting on the CS, $\mathbf{F}^{p1}$ includes the contact forces used to model the interaction between the new payload mass attached to the chain and the first bucket mass on the LS. Note that for the bucket closest to the anchor pulley, $\mathbf{F}^{i}_{tether}$ includes the force $-\mathbf{F}^{p1}$ due to the interaction between the bucket and the payload.

Equations 4 can be reduced to a form suitable for numerical integration:

$$\dot{\xi} = A\xi \tag{5}$$

where $\xi = \{u, \dot{u}\}$, and u is a vector containing the coordinates of the buckets, the CS and the first payload mass:

$$u = \left\{x_1, y_1, z_1, \ldots, x_n, y_n, z_n, x_{cs}, y_{cs}, z_{cs}, x_{p1}, y_{p1}, z_{p1}\right\}^T \tag{6}$$

The matrix A contains time-dependent terms due to inertial forces, gravitational forces and tension forces. Equation 5 can be numerically integrated in a given time range for a given initial state ξ_0. Integration is interrupted when a bucket reaches a pulley, to modify the direction of the velocity of the bucket intersecting the pulley. In particular, the following two cases are considered:

1) A bucket reaches the CS pulley. The payload mass m_p contained within the bucket is summed to the CS mass. The direction of the velocity of the bucket is then changed such that it is parallel to the vector connecting the CS with the first bucket on the DS closest to the CS. The velocity magnitude is not changed.
2) A bucket reaches the anchor pulley. Let i_0 be the index of this bucket. A payload mass m_p is connected to the i_0-th bucket via a spring-dashpot connection characterized by stiffness k and damping constant c. The direction of the velocity of the i_0-th bucket is then changed such that it is parallel to the vector connecting the anchor with the first bucket on the LS closest to the anchor. The velocity magnitude of the bucket is not changed. The spring-dashpot connection between the $(i_0 + 1)$-th bucket and the corresponding payload is removed, by fixing the payload to the bucket.

In the next sections the equations governing the gravitational potential and the tether forces are presented.

A. Asteroid gravitational environment

The asteroid is now modeled as a constant and uniform density triangular-faced polyhedron. This choice permits the model to resolve surface irregularities of an asteroid (e.g., cavities, craters or overhangs) and hence study the behavior of the orbital siphon in a general, non-spherical gravity field.

The polyhedron is defined by the coordinates of its vertexes and the connection topology, describing how the vertexes are connected with respect to each other. Werner and Scheeres [16] showed how the gravitational potential around a

constant density polyhedron and its gradient can be reduced to a summation over its edges and faces. Using dyadic notation these can be expressed as:

$$U(\mathbf{r}) = \frac{G\rho}{2}\left[\sum_{e\in\text{edges}} \mathbf{r}_e \cdot \mathbf{E}_e \cdot \mathbf{r}_e L_e - \sum_{f\in\text{faces}} \mathbf{r}_f \cdot \mathbf{F}_f \cdot \mathbf{r}_f \gamma_f\right] \tag{7}$$

$$\nabla U(\mathbf{r}) = -G\rho\left[\sum_{e\in\text{edges}} \mathbf{E}_e \cdot \mathbf{r}_e L_e - \sum_{f\in\text{faces}} \mathbf{F}_f \cdot \mathbf{r}_f \gamma_f\right] \tag{8}$$

where $G = 6.674\,28 \times 10^{-11}\ \mathrm{m^3\,kg^{-1}\,s^{-2}}$ is the gravitational constant, ρ is the density of the asteroid, $\mathbf{r}_e$ ($\mathbf{r}_f$) is a body fixed vector from any point on the edge (face) to the field point considered and the other parameters are defined in terms of the face geometry and orientation. Moreover, $\mathbf{E}_e$ and $\mathbf{F}_e$ are second order tensors depending on the properties of the edges and the faces, L_e is a quantity proportional to the length of each edge whereas γ_f is the solid angle associated with each face, as seen from the field point. For a triangular-faced polyhedron:

$$\mathbf{E}_e = \hat{\mathbf{n}}_f \hat{\mathbf{n}}_e^f + \hat{\mathbf{n}}_{f'} \hat{\mathbf{n}}_e^{f'} \tag{9}$$

$$\mathbf{F}_f = \hat{\mathbf{n}}_f \hat{\mathbf{n}}_f \tag{10}$$

$$L_e = \ln \frac{r_1^e + r_2^e + e_e}{r_1^e + r_2^e - e_e} \tag{11}$$

$$\gamma_f = 2\tan^{-1} \frac{\mathbf{r}_1^f \cdot \mathbf{r}_2^f \cdot \mathbf{r}_3^f}{r_1^f r_2^f r_3^f + r_1^f \mathbf{r}_2^f \cdot \mathbf{r}_3^f + r_2^f \mathbf{r}_3^f \cdot \mathbf{r}_1^f + r_3^f \mathbf{r}_1^f \cdot \mathbf{r}_2^f} \tag{12}$$

where $\mathbf{r}_j^f, (j = 1, 2, 3)$ are the position vectors from the field point to the face vertexes, taken in counter-clockwise order about the normal to the face, $\hat{\mathbf{n}}_f$, $\mathbf{r}_j^e, (j = 1, 2)$ are the two position vectors from the field point to the two edge vertexes, $\hat{\mathbf{n}}_e^f$ is a unit vector normal to the edge and to the corresponding face normal $\hat{\mathbf{n}}_f$, e_e is the length of the edge.

B. Tether tension forces

Let $\mathbf{q}_j$ be the relative displacement between the j-th and $(j+1)$-th mass of the chain, so that

$$\mathbf{q}_j = (x_{j+1} - x_j)\hat{\mathbf{i}} + (y_{j+1} - y_j)\hat{\mathbf{j}} + (z_{j+1} - z_j)\hat{\mathbf{k}}. \tag{13}$$

Here $\hat{\mathbf{i}}$, $\hat{\mathbf{j}}$ and $\hat{\mathbf{k}}$ are the unit vectors parallel to the x, y and z directions. Then, the tension forces $\mathbf{F}_j^s$ acting on the j-th mass are modeled according to Hooke's law, and therefore depend on the displacements $\mathbf{q}_j$ and $\mathbf{q}_{j-1}$:

$$\mathbf{F}_j^s = EA\epsilon_j \frac{\mathbf{q}_j}{|\mathbf{q}_j|} - EA\epsilon_{j-1} \frac{\mathbf{q}_{j-1}}{|\mathbf{q}_{j-1}|}. \tag{14}$$

Here, ϵ_j is the strain of the j-th tether, given by

$$\epsilon_j = \begin{cases} \dfrac{(|\mathbf{q}_j| - l)}{l} & \text{if} \quad |\mathbf{q}_j| > l \\ 0 & \text{if} \quad |\mathbf{q}_j| \leq l \end{cases} \tag{15}$$

Note that the tether cannot support axial compression thus the tension vanishes when the tether becomes slack.

If the j-th tether is in contact with one of the two pulleys, let $\mathbf{q}_j^a = \mathbf{r}_P - \mathbf{r}_j$ be the relative displacement between the j-th mass and the pulley, where $\mathbf{r}_P = \{x_P, y_P, z_P\}$ is the position vector of the pulley and $\mathbf{q}_j^b = \mathbf{r}_{j+1} - \mathbf{r}_P$ is the relative displacement between the pulley and the $(j+1)$-th mass. It is assumed that the tension on the j-th tether is constant between the two sections $\mathbf{q}_j^a$ and $\mathbf{q}_j^b$. Note that this is an approximation, as the pulley normally alters the tensions on the tether if friction at the tether-pulley interface is considered. Therefore, the assumption of a constant tension of the tether intersecting the pulley node is equivalent to assuming that the tether is sliding over the pulley. In this case the strain along the tether is given by

$$\epsilon_j = \frac{|\mathbf{q}_j^a| + |\mathbf{q}_j^b| - l}{l}. \tag{16}$$

C. Tether damping forces

It is assumed that the damping forces are proportional to the strain rate $\dot{\epsilon}_j$. From Eq.(15) it can be shown that:

$$\dot{\epsilon}_j = \begin{cases} \dfrac{\dot{\mathbf{q}}_j \cdot \mathbf{q}_j}{|\mathbf{q}_j| l} & \text{if} \quad |\mathbf{q}_j| > l \\ 0 & \text{if} \quad |\mathbf{q}_j| < l \end{cases} \tag{17}$$

where

$$\dot{\mathbf{q}}_j = (\dot{x}_{j+1} - \dot{x}_j)\hat{\mathbf{i}} + (\dot{y}_{j+1} - \dot{y}_j)\hat{\mathbf{j}} + (\dot{z}_{j+1} - \dot{z}_j)\hat{\mathbf{k}} \tag{18}$$

Then, the total damping force contribution to the motion of the j-th mass is given by

$$\mathbf{F}_j^d = C\dot{\epsilon}_j \frac{\mathbf{q}_j}{|\mathbf{q}_j|} - C\dot{\epsilon}_{j-1} \frac{\mathbf{q}_{j-1}}{|\mathbf{q}_{j-1}|} \tag{19}$$

If the j-th tether is in contact with one of the two pulleys, the strain rate $\dot{\epsilon}_j$ is obtained by taking the time derivative of Eq. (16), under the assumption that the damping force remains constant over the tether crossing the pulley:

$$\dot{\epsilon}_j = \frac{1}{l}\left[\frac{\mathbf{q}_j^a \cdot \dot{\mathbf{q}}_j^a}{\left|\mathbf{q}_j^a\right|} + \frac{\mathbf{q}_j^b \cdot \dot{\mathbf{q}}_j^b}{\left|\mathbf{q}_j^b\right|}\right] \tag{20}$$

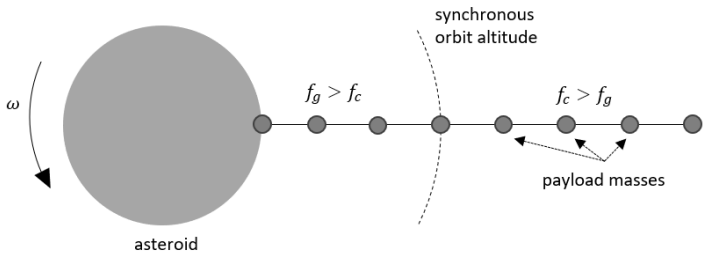

Fig. 2 Simplified orbital siphon model, as studied in [14].

Then, the total tether force acting on the j-th mass is the sum given by

$$\mathbf{F}^j_{tether} = \mathbf{F}^s_j + \mathbf{F}^d_j \tag{21}$$

D. Tether forces on the collecting spacecraft

The dynamics of the CS is governed by Eq. (4b). Using the notation introduced above, the force $\mathbf{F}^{CS}_{tether}$ acting on the CS is written as

$$\mathbf{F}^{CS}_{tether} = (EA\epsilon_j + C\dot{\epsilon}_j)\frac{\mathbf{q}^b_j}{|\mathbf{q}^b_j|} - (EA\epsilon_j + C\dot{\epsilon}_j)\frac{\mathbf{q}^a_j}{|\mathbf{q}^a_j|} \tag{22}$$

where the index j in this case refers to the tether in contact with the pulley. Note that any other external force generated by the contact between the released material and the CS is neglected.

E. Orbital siphon effect

Consider the simplified model shown in Fig.2, (as the one studied in [14]), where a chain of masses is anchored at the equator of a spherical asteroid, with the masses aligned and normal to the asteroid surface and extending beyond the synchronous orbit radius. For simplicity any distinction between 'payloads' and 'buckets' is here avoided and the term 'mass' is used to indicate an element of the chain. Each mass will experience gravitational and centrifugal-induced forces, in addition to the internal forces from its nearest neighbors in the chain. The gravitational force will be larger than the centrifugal-induced force for masses below the synchronous orbit radius and *viceversa* for masses above it. For an adequate number of masses and spacing between them, the chain can be configured to remain in equilibrium. If the chain is extended beyond such an equilibrium configuration there will be an excess of centrifugal-induced force acting on the masses above the synchronous orbit radius and the chain is lifted. An orbital siphon effect can be established if new masses are connected at the bottom of the chain and the upper masses are released. The excess of centrifugal force implies a constant acceleration of the chain. However, it has been shown in [14] that the momentum exchange between the mass to be connected (initially at rest) and the rest of the chain eventually leads the siphon to reach the steady state

Table 1 Physical properties of Bennu and Golevka and polyhedra details. Shape models are taken from [17, 18].

	Bennu	Golevka
Period [18, 19]	4.297 h	6.0289 h
Density [19, 20]	1.26 g cm^{-3}	2.7 g cm^{-3}
Equivalent sphere radius	246 m	265 m
Polyhedron vertexes	1348	2048
Polyhedron faces	2692	4092

velocity:

$$v_{\max} = \omega R \left(\frac{L}{2R} \left[2 + \frac{L}{R} - \frac{2}{\left(1 + \frac{L}{R}\right)} \left(\frac{\omega^2}{\frac{4}{3} G\pi\rho} \right)^{-1} \right] \right)^{1/2} \tag{23}$$

where R is the radius of the asteroid.

Similarly, for the bucket conveyor model studied here, if the structure is long enough, the excess of centrifugal-induced force on the LS will induce a rotation of the chain with respect to the pulleys and an orbital siphon effect is established when payloads are released to the CS. Buckets are recycled through the DS and the LS is populated with new payloads as empty buckets reach the anchor pulley. Contrary to the model used in Ref. [14], no support structure is envisaged here and the chain does not rotate as a rigid body. However, it will be shown not only that the siphon reaches a finite steady state speed as in Ref. [14], but also that such speed can be accurately predicted by Eq. (23)

III. Simulated case studies

Simulations are now performed considering the two near-Earth asteroids 101955 Bennu and 6489 Golevka. The physical properties and details of the polyhedral models used are given in Table 1. Figure 3 shows the shape models of the two asteroids. Bennu has a spinning top-shape and a ridge along the equatorial region. Bennu is the 4-th most profitable known asteroid for mining purposes [*] within the near-Earth asteroid population. Golevka has a more irregular shape and hence it represents an interesting case study for the orbital siphon, to understand how the gravitational field influences the siphon dynamics.

It is assumed that both asteroids are principal axis rotators [19, 21], i.e., their angular velocity vector is aligned with their maximum moment of inertia axis (here the z axis) and therefore maintain a constant angular velocity in the absence of external torques. Precession and nutation are neglected as the majority of asteroids in a complex rotational state are characterized by a slow rotational rate [22] (unlike Bennu and Golevka) and therefore are not suitable for this application: a slow rotation rate would be associated with very large orbital siphon structures [14].

Figure 4 shows the magnitude of the effective acceleration $|\nabla V|$ on the surface of the two asteroids. For Bennu the effective acceleration is larger at the poles and lower at the equatorial region (this trend is typical for spheroidal asteroids).

[*] According to *asterank.com* (Date accessed: 11/10/2019)

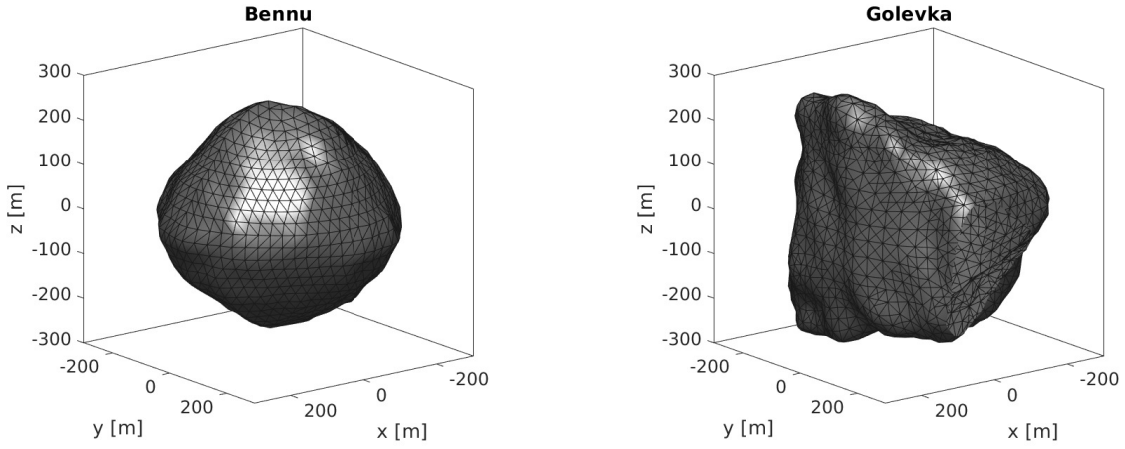

(a) (b)

Fig. 3 Shape models for Bennu (3a) and Golevka (3b).

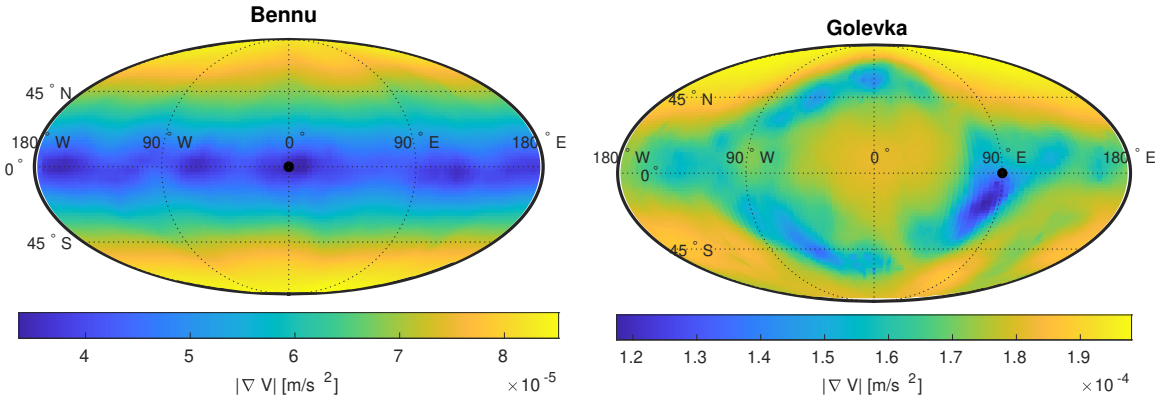

(a) (b)

Fig. 4 Effective acceleration $|\nabla V|$ at the surface of Bennu (a) and Golevka (b). A black circle indicates the selected anchor location for the two bodies.

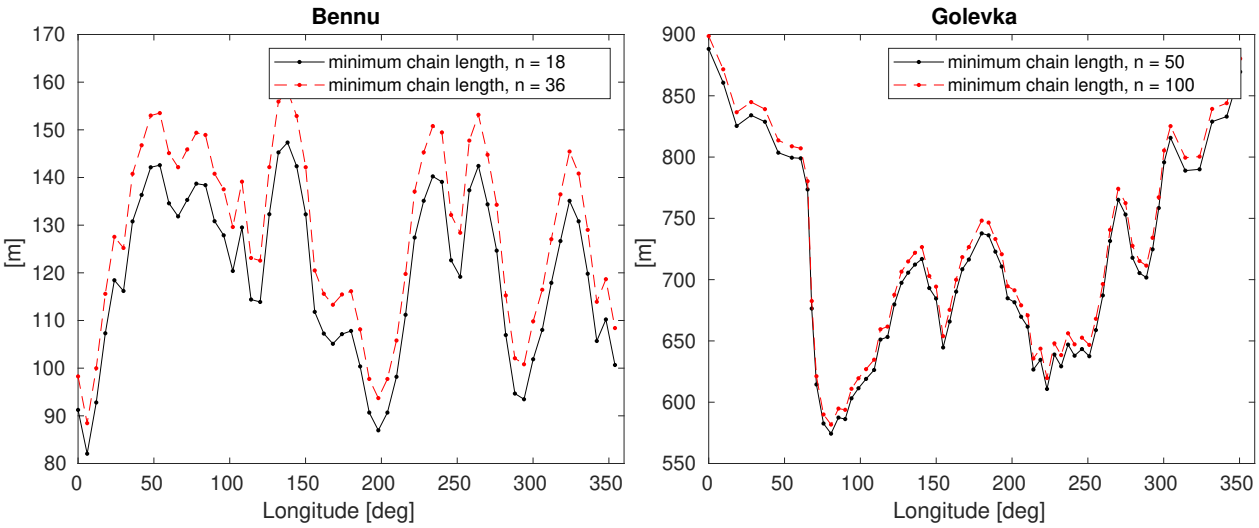

(a) (b)

Fig. 5 Equilibrium length of equatorial chains anchored on Bennu (a) and Golevka (b) as a function of the anchor longitude and the number of buckets.

In fact, close to the poles, the centrifugal-induced acceleration is small and thus the gradient of the effective potential V is mainly influenced by the gravitational field. Moving away from the poles, the centrifugal-induced acceleration increases, thus competing with the gravitational acceleration and reducing $|\nabla V|$. The map of $|\nabla V|$ does not follow the same pattern on the surface of the asteroid Golevka, due to its more irregular shape. The acceleration is minimized in a region close to 90 deg longitude at the equator and is larger at the north pole. Although not directly represented here, the vector ∇V points inward across the surface of both asteroids.

The effective acceleration is related to the minimum length (here called *equilibrium length* in analogy with [14]) the siphon must have to guarantee the siphon effect. Figure 5 shows the equilibrium length for Bennu (5a) and Golevka (5b) for equatorial anchor positions, as a function of the anchor longitude and the number of payload masses. Here the equilibrium length is calculated assuming that the two sides of the chain are coincident and normal to the z axis. Note that equatorial regions with smaller equilibrium lengths are also characterized by a smaller effective acceleration at the surface (see Fig. 4). The anchor longitude which minimizes the equilibrium length is approximately 6 deg for Bennu and 80 deg for Golevka. Larger siphon lengths are required for Golevka due to its larger density and rotation period (in fact, the effective acceleration for Golevka is on average one order of magnitude larger than Bennu). Note that the equilibrium length decreases with more buckets. This is consistent with results found in [14]. It is important to emphasize that the equilibrium length will change depending on the current chain configuration. Values shown in Fig. 5 are used as a reference for the selection of suitable chain lengths for the following case studies:

Scenario 1. Bennu: orbital siphon with a fixed anchor. The simulations are performed for three cases, varying the siphon length and/or payload mass

Case (1): $m_p = 34\,\text{kg}$, $L = 99\,\text{m}$,

Case (2): $m_p = 126\,\text{kg}$, $L = 99\,\text{m}$,

Case (3): $m_p = 34\,\text{kg}$, $L = 124\,\text{m}$.

The number of buckets n is set to 35. The two different payload masses correspond to the mass of asteroid material which can be filled in a cubic bucket with size 30 cm or 46 cm. The bucket mass is calculated assuming the bucket is made of Aluminium 7075-T6 with a density of $2.81\,\text{g}\,\text{cm}^{-3}$ and each face has a thickness of 1 mm. This leads to $m_b = 1.5\,\text{kg}$ for the smaller bucket and $m_b = 3.5\,\text{kg}$ for the larger bucket. The orbital siphon is anchored at 0 deg longitude at the equator. Note that both the siphon lengths used in this scenario are larger then the equilibrium length for this longitude, as shown in Fig. 5a. In all cases the initial mass of the CS is assumed to be 800 kg.

Scenario 2. Golevka: orbital siphon with a fixed anchor at 90 deg longitude at the equator. A 595 m chain with 105 payloads is used for the simulation. Again, note that such a length is larger than the equilibrium length shown in Fig. 5b for an equatorial siphon at the indicated longitude. A 30 cm side cube is used for this simulation, corresponding to a payload mass $m_p = 73\,\text{kg}$ (note that in this case more mass can be filled in the 30 cm bucket due to the larger density of Golevka). In this case two scenarios are studied, to analyze the effect of the CS mass at the beginning of the mass transfer process:

Case (1): $m_{cs}(t = 0) = 1600\,\text{kg}$,

Case (2): $m_{cs}(t = 0) = 2400\,\text{kg}$.

Scenario 3. Bennu: orbital siphon with moving base. The siphon base undergoes a constant velocity motion on the asteroid surface, for example to move to a new mining location without interrupting the flow of transported material. The initial base point is the same as Scenario 1 and two cases are here considered:

Case (1) Longitudinal motion of the anchor base, with siphon length 99 m. The anchor is moved by 60 m along the positive y direction, with constant anchor velocity $1 \times 10^{-3}\,\text{m}\,\text{s}^{-1}$.

Case (2) Latitudinal motion of the anchor base, with siphon length 124 m. The anchor is moved by 30 m along the positive z direction, with constant anchor velocity $1 \times 10^{-3}\,\text{m}\,\text{s}^{-1}$.

In both cases the payload mass is 34 kg and the initial mass of the CS is 800 kg.

The siphon is initialized by arranging the LS and DS buckets starting from the anchor point and following a straight line, parallel to the segment OA, with the first bucket coincident with the anchor point. The siphon initial deployment and LS loading are not taken into account here: the LS buckets are already loaded with payloads at the beginning of the simulation. All the buckets are initialized with zero velocity. In each simulation, the tether stiffness and damping are $EA = 21\,100\,\text{N}$, $C = 2500\,\text{N}\,\text{s}$ (values taken from Reference [9]), while $k = 300\,\text{N/m}$ and $c = 200\,\text{Ns/m}$.

The siphon orientation is measured with respect to the CS (in general the chain shape will deform in the three dimensional space), using the local azimuth and elevation defined as in Fig. 6. Note that the elevation is defined with

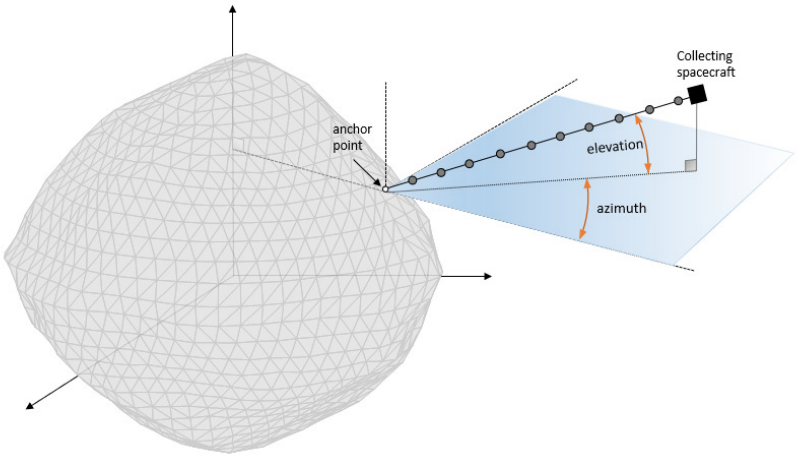

Fig. 6 Definition of azimuth and elevation angles, used to define the orientation of the CS with respect to the anchor point. For illustration, the siphon is represented here as a straight line.

respect to the the plane passing through the anchor point and normal to the spin axis (which corresponds to the equatorial plane in Scenarios 1, 2 and 3a).

In all simulations the asteroid mass is considered constant and the effects of long-term mass removal are not taken into account, since the removed mass fraction is small.

IV. Results

Scenario 1. Figure 7 shows the CS azimuth, CS elevation, CS distance from the anchor, average chain velocity (defined as $(1/n)\sum_{i=1}^{n}|\dot{\mathbf{r}}_i|$) and the z coordinate of bucket #1 for a 28 h simulation, for each case considered. The Coriolis forces due to the chain motion initially cause a clockwise rotation of the chain (opposite to the asteroid rotation) and the amplitude of such oscillations is eventually reduced over time (Fig. 7a). A similar trend can be observed for the CS elevation (Fig. 7b). The variation of the CS elevation is due to the irregularities of the gravitational field, especially in close proximity to the asteroid, where buckets are deflected in the z direction (see also Fig. 7e) and the consequent oscillation is propagated to the other buckets of the chain and eventually to the CS.

The average chain speed (Fig. 7e) reaches a steady value after an initial transient. The radial deceleration is due to payload refilling and is similar to the effect described in References [14, 15] and recalled in Sect. II.E: when a new payload mass is added at the bottom of the siphon, this mass is accelerated by the bucket while the average chain speed decreases to conserve the linear momentum of the system. Hence, although the uppermost masses of the LS are generating a net radial force, the average chain speed does not diverge, due to the deceleration phase caused by bucket refilling. Such a braking effect introduces elastic forces on the siphon, which are propagated along the entire chain. The higher frequency variations on the average chain speed are a consequence of this effect. The dashed line in

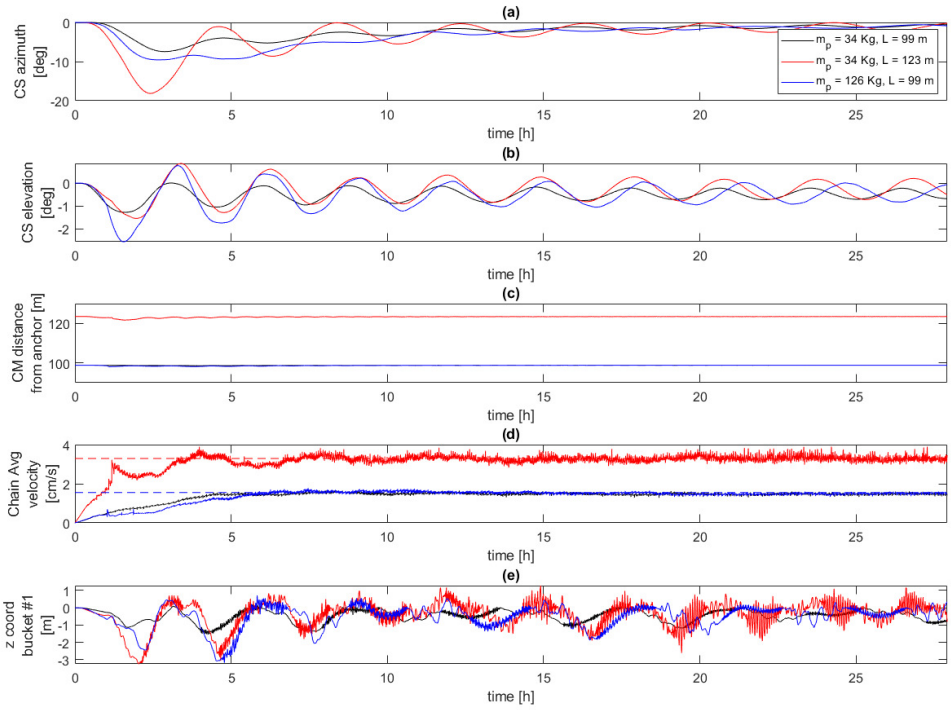

Fig. 7 Scenario 1: CS azimuth (a), CS elevation (b), CS distance from anchor (c), chain average velocity (d) and z-coordinate of bucket #1 (e) as a function of time.

Fig. 7 represents the steady state speed predicted by the analytical model in [14], using Eq. (23) [†]. This matches quite accurately the average chain speed after approximately 10 hours of simulation time in all cases.

Figure 8 is a view of the siphon from the positive z axis at the beginning of the fourth, fifth and sixth loop of the chain (the chain completes a *loop* when bucket #1 reaches the anchor after completing an entire ascent on the LS and descent on the DS) for Scenario 1, Case (1). The siphon is transversally stretched, due to the opposite direction of the Coriolis forces on the two sides of the chain, which contributes to keep the two sides separated. It has been verified that buckets on opposite sides do not collide.

Figure 9 shows the tension force on the tether connecting bucket #1 with bucket #2 during the third loop of the chain for all three cases. Overall, the tension force is very small, less than 0.2 N on average and with peaks below 2 N for Scenarios 2 and 3. The peaks are associated with a new payload being attached to the bucket entering the LS: this can cause the tether to lose tension and become slack, even though the overall stability of the analysed scenarios is not compromised. The amplitude of the peaks depends on the current configuration of the chain. In general, the tension force on the tethers increases for larger chain length or payload mass.

[†]Here, the radius R and ω of the spherical asteroid (used in Eq. (23)) are chosen such that the gravitational acceleration and the centrifugal-induced acceleration are matching with that of the polyhedron model at the anchor point.

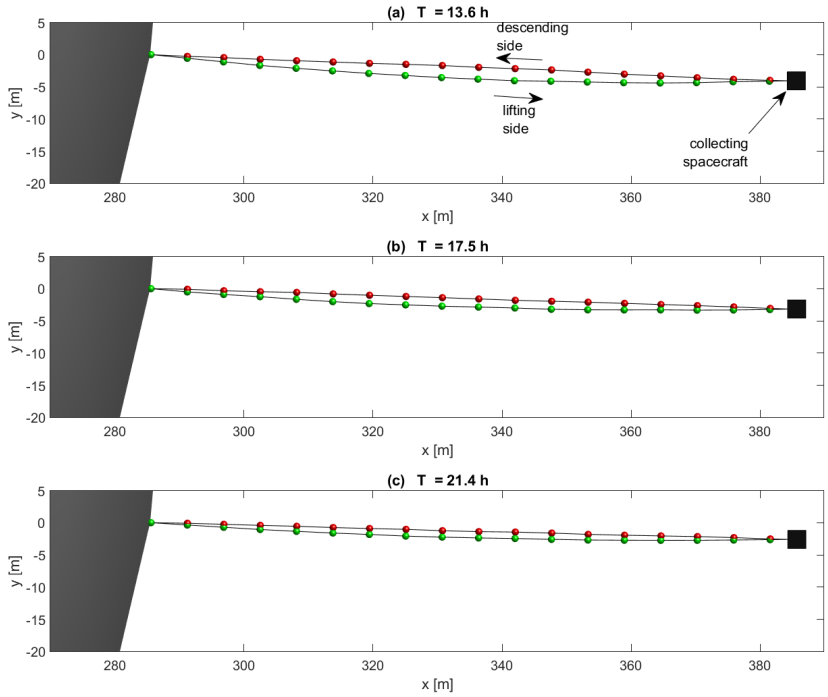

Fig. 8 Scenario 1, case (1): orbital siphon as viewed from the positive z axis.

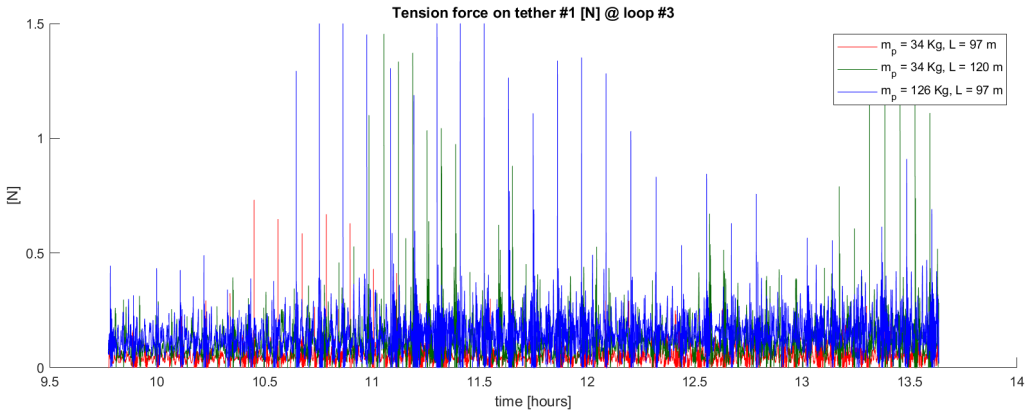

Fig. 9 Tension force on the tether #1 during the third loop of the chain for the three cases in Scenario 1.

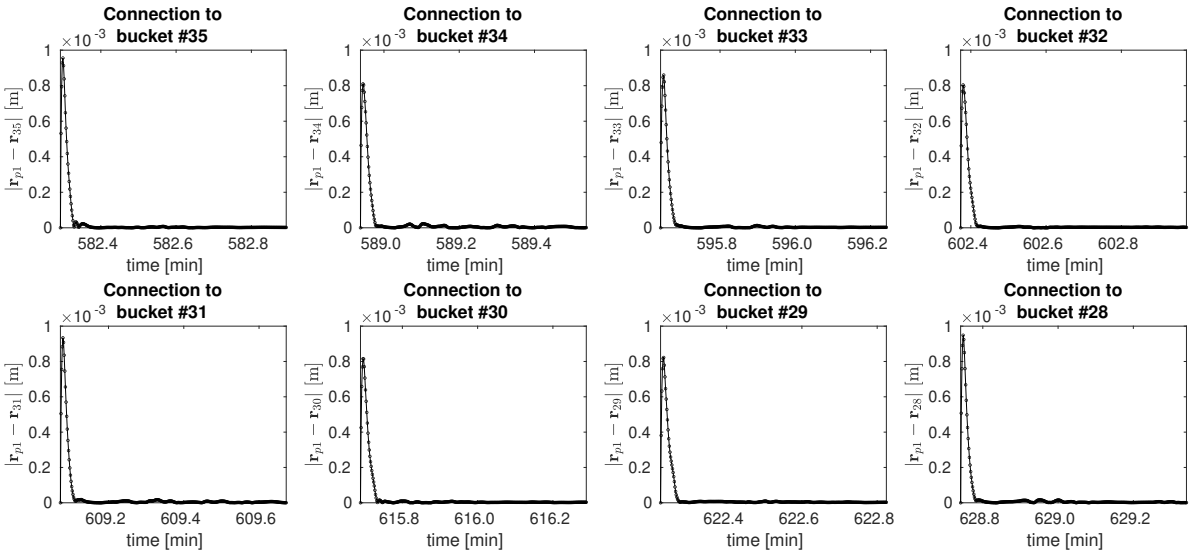

Fig. 10 Relative position between new payload and bucket after connection. Connections of the first eight payloads at the beginning of the third cycle are shown.

Figure 10 shows the magnitude of the relative position between the new payload and the bucket after connection at the anchor. Connection of the first eight payloads at the beginning of the third cycle is displayed here as reference: the other cases exhibit equivalent characteristics. After an initial peak, corresponding to the payload being accelerate by the chain, oscillations are damped within a few seconds after the connection.

Scenario 2. Figure 11 shows the CS azimuth, CS elevation, CS distance from anchor, average anchor speed and the z coordinate of bucket #1 for a 50 h simulation, in the two cases considered.

Again, as in the previous scenario, the siphon rotates clockwise, opposite to the asteroid rotation, due to the Coriolis forces. After an initial transient, the CS azimuth is reduced and the chain tends to approach the local vertical (see also Fig. 12). It is interesting to observe that the variation of the CS elevation is rather small, although the asteroid shape is quite irregular. Therefore, it is plausible that the centrifugal-induced forces on the uppermost payloads are large enough to counteract the z component of the gravitational force on the lowermost masses. The difference between Scenario 2, Case (1) and Scenario 2, Case (2) is not significant. The CS elevation in the case (2) is slightly smaller in amplitude, due to the larger centrifugal-induced force available at the CS.

Figure 12 is a view of the siphon from the positive z axis at different timesteps for Scenario 2, Case (1). The situation here is analogous to Fig. 8. In this case, the transversal stretching is larger at the beginning but is reduced over time. No collision between buckets on opposite sides was detected for these simulations.

Scenario 3 - Siphon with moving base. Figure 13 shows the CS azimuth, CS elevation, average anchor velocity and the z coordinate of bucket #1 for a 58 h simulation of Scenario 3, Case (1) and Scenario 3, Case (2). The dotted vertical

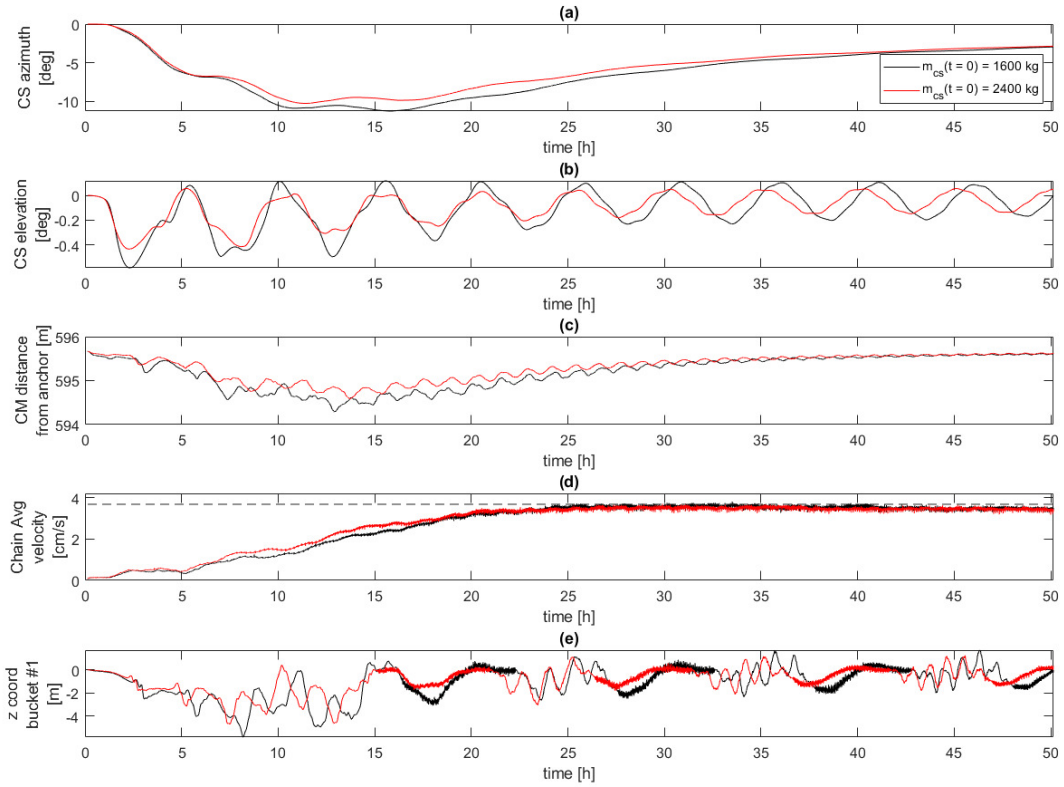

Fig. 11 Scenario 2: CS azimuth (a), CS elevation (b), chain average velocity (c) and z-coordinate of bucket #1 (d) as a function of time.

lines mark the interval when the siphon base is moving.

For the longitudinal base motion, the siphon changes its orientation to follow the direction of the centrifugal-induced force, which is parallel to the vector OA. The chain average velocity is larger during the base motion phase and then reduces once the base is fixed. The larger chain velocity is due to the additional centrifugal-induced force caused by the moving anchor. The amplitude of the CS azimuth is reduced over time once the siphon base is fixed.

When the anchor is moving towards the positive z axis a significant change is noted in the CS elevation: the chain bends slightly southward (see Fig. 13b and Fig. 15). This effect is caused by the misalignment between the gravitational force and the centrifugal-induced force when the anchor moves northwards: the centrifugal-induced force on each bucket will keep the siphon perpendicular to the spin axis whereas the gravitational force is (approximately) pointing towards the asteroid center-of-mass, thus their sum has a net negative (positive if the siphon was moving southward) z component. This same effect has been noted in Reference [23], where the static behaviour of a non-equatorial space elevator was analysed for Earth applications.

Figures 14 and 15 show the siphon at four different times during the simulation. Note from Fig. 14 that the siphon

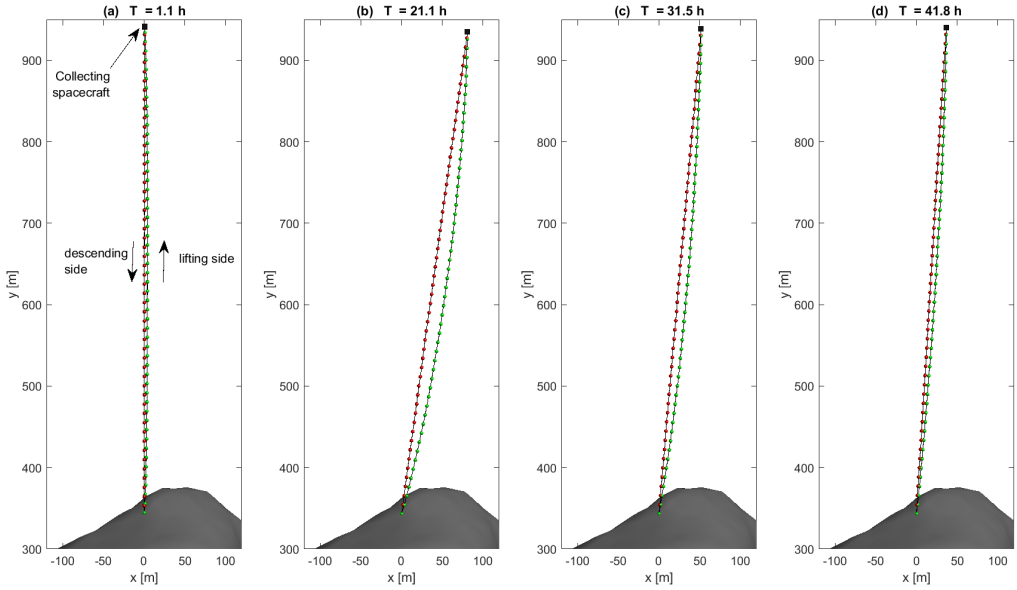

Fig. 12 Scenario 2, Case (1): orbital siphon as viewed from the positive z axis.

orientation adjusts during the anchor motion to follow the radial direction of the centrifugal-induced force. Moreover, for latitudinal motion, the bending effect is evident from Fig. 15. No collision was detected between buckets on opposite sides.

It should be noted that the speed of the anchor is about one order of magnitude smaller with respect to the average chain speed in the cases simulated here. It is plausible that, for a larger anchor speed, the average chain speed will increase even further during the motion phase, possibly introducing instabilities and/or collision between buckets on opposite sides.

V. Discussion

Following the results, two key remarks can be made. First, stability of the orbital siphon is possible when the siphon is anchored at an irregularly shaped asteroid. This result is consistent with [24] where oscillations of a tether attached to an irregularly shaped celestial body were studied, taking into account C_{20} and C_{22} in the spherical harmonic expansion of the gravitational potential. Secondly, the siphon effect can be generated using a self-supporting tether-structure, without the payloads sliding on a rigid rod or a support tether: such a siphon architecture reduces the scale of infrastructure mass with respect to a siphon with support structure. Moreover, the lifting side and descending side of the siphon do not interfere or touch in all the cases presented here, due to the opposite direction of the Coriolis forces on the two sides.

The siphon dynamics can be divided in two phases: a transition phase and a steady state phase. During the transition phase the chain accelerates and the siphon rotates with respect to the anchor point. A key aspect of this phase is the

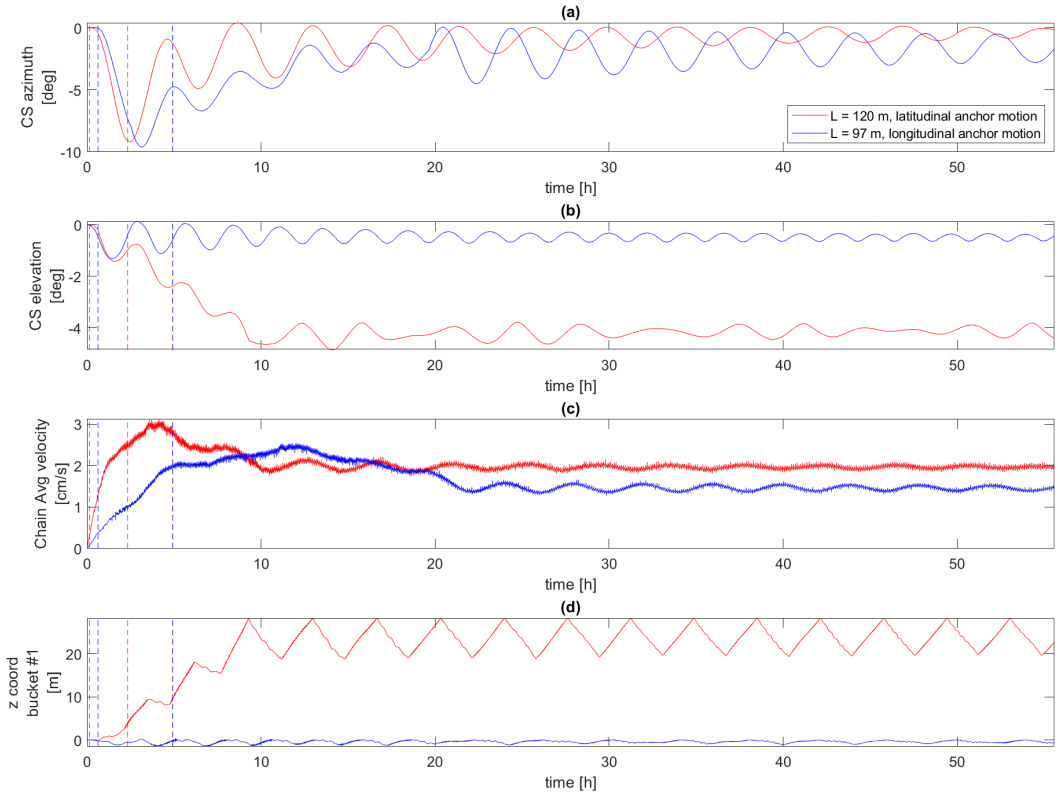

Fig. 13 Scenario 3, Case (1) (blue) and Scenario 3, Case (2) (red): CS azimuth (a), CS elevation (b), chain average velocity (c) and z-coordinate of bucket #1 (d) as a function of time. The dotted vertical lines mark the interval when the siphon base is moving.

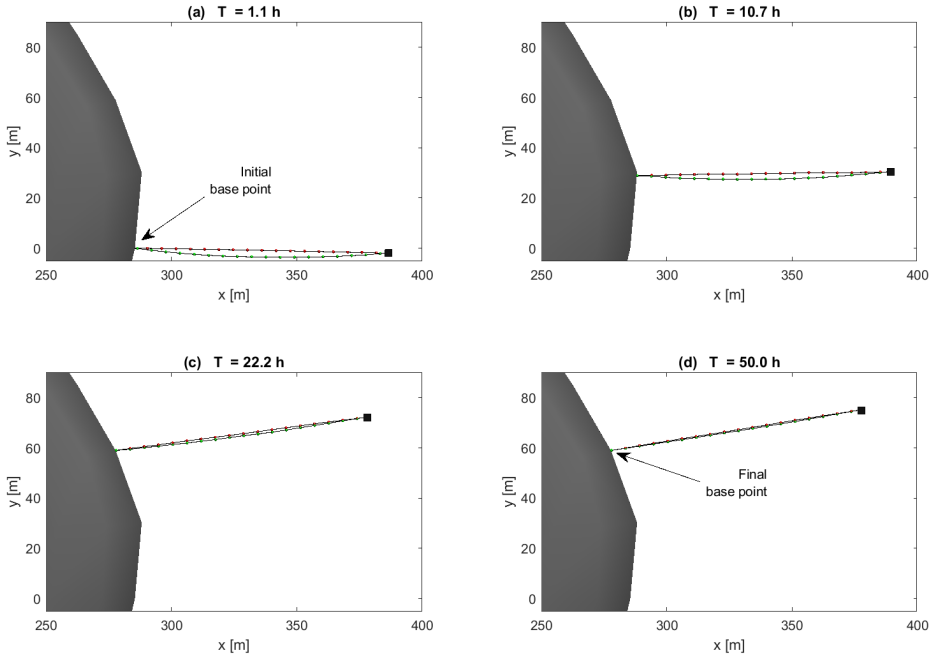

Fig. 14 Scenario 3, Case (1): orbital siphon as viewed from the positive z axis.

progressive reduction of the siphon azimuth, with the chain gradually aligning with the local vertical. This effect was also observed in previous models [14, 15] that studied the siphon rotation with payload masses constrained to slide along a rigid support. It is observed in [15] that, the siphon oscillates about an axis, passing through the anchor, where the net torque produced by the inertial and external forces with respect to the anchor cancels out. Here, although the siphon is non-rigid, the dynamics appears similar. The Coriolis forces generate a net clockwise torque, shifting the equilibrium towards negative azimuth values. The equilibrium axis then asymptotically approaches the direction of zero azimuth as more mass is delivered to the CS and the torque produced by the centrifugal forces on the CS with respect to the anchor point counteracts the Coriolis torque. The reader is referred to [25] for additional details. In the following steady-state phase the average chain speed reaches an asymptotic value (small oscillation are still observed here mainly due to undumped motion in the z direction). This steady state speed matches quite accurately the value predicted by Eq. (23), which was derived in [14] for a siphon with payloads sliding on a non-rotating structure and ranges from 2 to 4 cm s^{-1} for the two scenarios presented here.

Although seemingly small, the mass flow rate of material delivered to the CS, can be increased by using larger payload masses. For example, using a 34 kg payload mass on Bennu the average mass flow rate is 288 kg/hr (Scenario 1, Case (1)), whereas for a 126 kg payload mass the mass flow rate raises to 1005 kg/hr (Scenario 1, Case (2)). One of the major disadvantages of large payload masses is the larger bucket volume required to host the material (in relation to the asteroid material density), which increases the structural mass of the siphon and hence the costs to deliver the

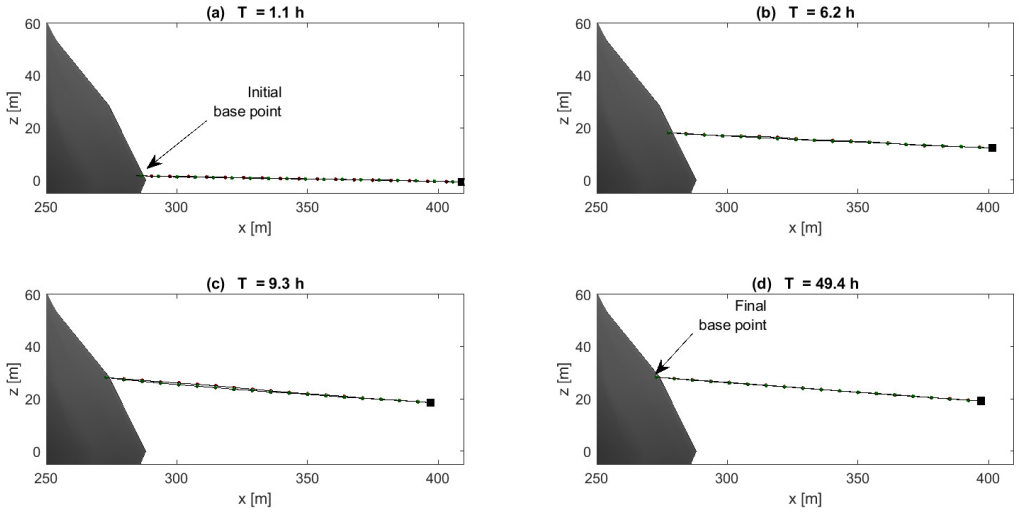

Fig. 15 Scenario 3, Case (2): orbital siphon as viewed from the negative y axis.

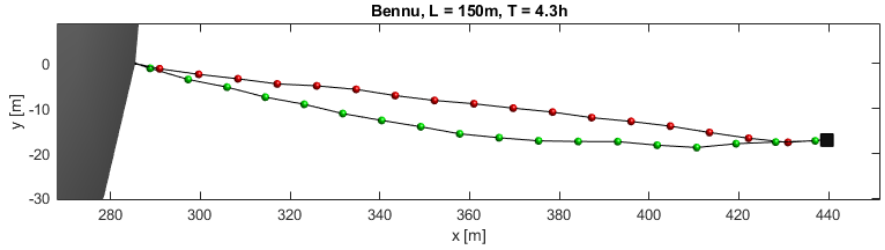

Fig. 16 Interference between LS and DS for a siphon anchored at Bennu with length $L = 150\,\mathrm{m}$ and other parameters as in Scenario 1. Top view from the positive z axis.

infrastructure material to the asteroid. Other possible drawbacks of larger buckets are related to the bucket-cable attachment, and the sliding motion of the cable through the two pulleys in case of larger attachments. Further studies are required to investigate these engineering issues in detail.

By using longer siphons the average speed of the chain increases (compare case 1 and 2 in Scenario 1), as the chain will benefit from larger centrifugal-induced force on the uppermost masses, thus in principle increasing the mass flow rate. However, it has been observed that if the chain length increases after a certain threshold (which depends on the asteroid, anchor location and tether properties) the two sides of the chain can interfere causing unwanted bucket collision. Figure 16 shows an example of a siphon with length $L = 150\,\mathrm{m}$ anchored at Bennu, with other parameters as in Scenario 1. The LS and DS side are interfering in proximity of the CS. This problem may be circumvented by dissipating residual oscillation through dampers located in proximity to the anchor and the CS. However, a laterally constrained siphon would not experience this issue, as any oscillation in a direction perpendicular to the structure would be damped by the structure itself, without propagating through the chain.

For the chain velocities considered here, the tension on the tethers is of the order of 1 N. The small magnitude of the tension force is a consequence of the small length-scale of the structure involved, when compared to similar concepts applied at larger scales such as the *space elevator* for terrestrial applications.

The required anchor forces have the same order of magnitude as the tether forces. According to recent work on anchor mechanisms for asteroid landing and mining operations, proposed anchoring devices can withstand much larger forces. For example, *area-of-effect softbots* [3] are soft-robotic spacecrafts with a large and flexible surface area to exploit the dynamical environment at rubble pile asteroids: a $1\,\mathrm{m}^2$ softbot can generate a 10 N net force to remain anchored to the asteroid surface [3]. Other recent research on asteroid landing [26] compares the behaviour of different anchor tips in different media, claiming anchor forces between 36 N and 178 N.

The dynamics of a siphon with a moving base was also investigated. In particular, the behaviour of a siphon undergoing small longitudinal and latitudinal anchor displacement on the surface of the asteroid Bennu has been analyzed. For a small base velocity ($1 \times 10^{-3}\,\mathrm{m\,s^{-1}}$) a siphon undergoing longitudinal motion tends to remain parallel to the radial direction defined by the centrifugal-induced force. Latitudinal surface motion causes a significant change of the CS elevation (Fig. 15), due to the misalignment between the gravitational force and the centrifugal-induced force. In both cases, the siphon has to be long enough to generate the orbital siphon effect at the desired final anchor location.

A siphon with a moving base may be a convenient solution to move the entire infrastructure to a different mining location without interrupting the delivery of material to the CS. However, this scenario calls for several engineering challenges. Among them is the efficient locomotion of the base on the asteroid surface, which is clearly influenced by small-scale surface features, e.g. boulders or cavities. An interesting solution is the recent *grappler* concept proposed in Reference [27]. The key idea is to create a net-like mechanism by connecting multiple bi-stable array elements (called grapplers) that would grip variable asteroid terrain. In this case, the siphon base would move along an articulated structure defined by multiple grapplers adhering to the asteroid surface. The small siphon anchoring force requirements make the grapplers a viable solution to address the problem of a siphon with moving base.

The power requirements to perform locomotion manoeuvrers on the surface will depend in general on the projection of the anchor force on the anchor velocity direction, the magnitude of the anchor velocity and any friction involved. Neglecting friction, in principle an anchor force of 1 N [‡] in the direction of motion requires a power of 1×10^{-3} W to move the siphon at a speed of $1 \times 10^{-3}\,\mathrm{m\,s^{-1}}$.

A. Deployment, operation and braking

Another significant engineering challenge is the deployment of the orbital siphon system. A proposed deployment scenario (see Fig. 17) is to station the CS in proximity to an equilibrium point around the asteroid (a) and then deploy

[‡]Note that, in general, the component of the anchor force in the direction of anchor motion will be much smaller than the component normal to the asteroid surface.

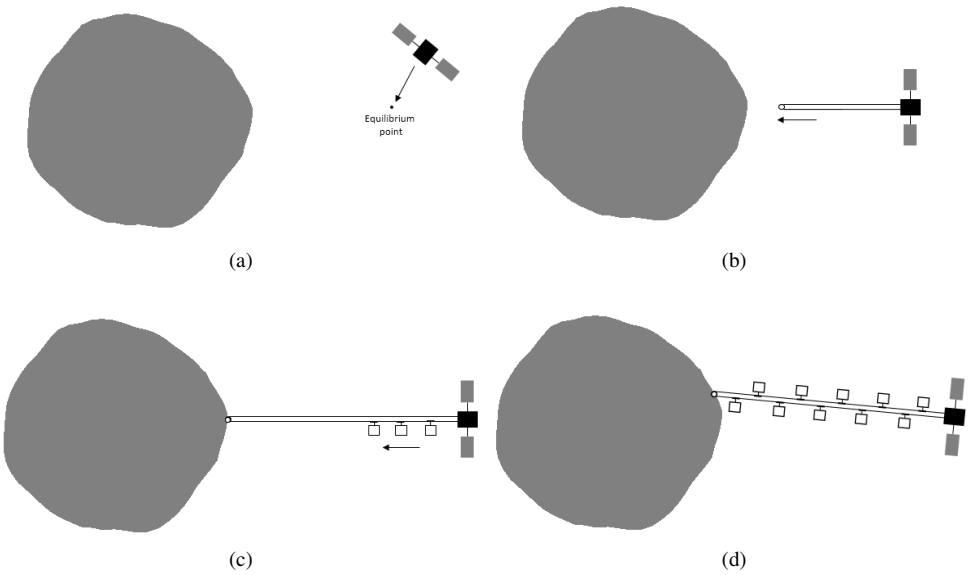

Fig. 17 Concept of system deployment. (a) The CS approaches one of the asteroid equilibrium points. (b) The tether system is released. (c) Anchoring and bucket attachment (d) Buckets on the LS are filled with payload material.

the tether to the surface (b). The tether is then anchored to the surface (c). To avoid deflection caused by inertial forces during the tether deployment, motion control is required in this phase, for example by using a propulsion system attached at the bottom of the tether. If a net-like structure is to be used to control the locomotion of the siphon base on the asteroid surface, this has to be landed in advance: the siphon anchoring device would then be attached to the grappler system. Once the anchor is fixed, the CS is raised to reach the desired siphon length. Buckets are attached to the tether by cycling the tether using external torque applied to the pulleys. In this phase, the siphon structure can be exploited to land mining equipment (e.g., mining rovers) onto the surface. The LS of the siphon is then filled with material. When all the LS buckets are filled with payloads, the orbital siphon effect is initialized and the anchor base is translated to the desired location (d).

The nominal mass flow rate of the siphon is constrained by the technology available for the surface miners. These would transfer material to the siphon base for bucket refilling. The ability to extract large quantities of regolith with a large number of surface miners clearly increases the mass flow rate of material that can be delivered to the CS.

The centrifugal-induced force generated by the rotation of the bucket on the upper pulley can be exploited to transfer the payload material to the CS. Figure 18 shows the proposed concept for material release, which is only mentioned here and a detailed analysis is left for future work. A conical hopper attached to the CS is envisaged to collect the material once released by each bucket. The centrifugal-induced force acting at the CS altitude will then cause material migration towards the convergent end of the hopper, after material is released.

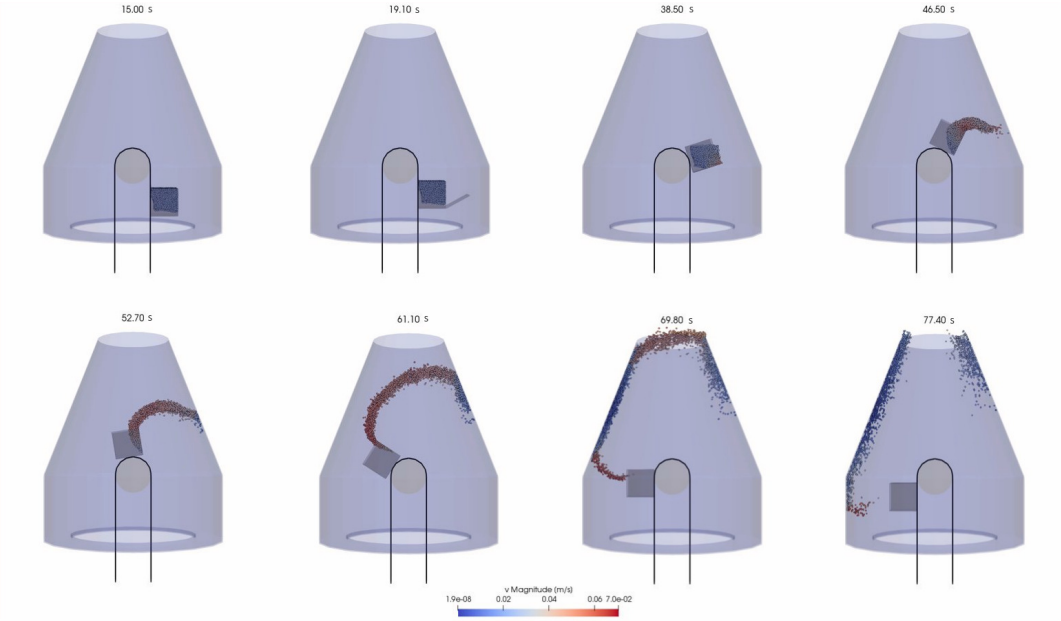

Fig. 18 Release of material on the CS collector.

B. Effect of solar perturbations

A concern that might arise is whether the siphon dynamics is influenced by the solar gravitational perturbation or the solar radiation pressure. The radius of the sphere of influence of the asteroid can be approximated by [28]

$$r_{\text{soi}} = a\left(\frac{M}{M_{\odot}}\right)^{2/5} \tag{24}$$

where a is the semimajor axis of the orbit of the asteroid, M is the asteroid mass and $M_{\odot}$ is the mass of the Sun. Then, for the asteroids Bennu and Golevka, the radius of the sphere of influence calculated with Eq. (24) is, respectively 3 km and 9.6 km. The siphon lengths chosen for this simulations are well within the sphere of influence in both cases. It is therefore plausible that the Sun's third-body perturbation will not significantly alter the dynamics of the system.

A simple solar radiation model is used to evaluate the effect of the solar radiation pressure on the CS. Assuming the CS presents a constant area perpendicular to the Sun-line, the net acceleration a_{SRP} acting away from the Sun-line has magnitude [22]:

$$a_{\text{SRP}} = \frac{(1+\eta)P_0}{Bd^2} \tag{25}$$

where B is the mass-to-area ratio B of the CS and η its reflectivity; $P_0 = 1 \times 10^8\,\text{kg}\,\text{km}^3\,\text{s}^{-2}\,\text{m}^{-2}$ is a constant related to the magnitude of the solar radiation pressure and d is the distance of the asteroid with respect to the Sun. The spacecraft mass-to-area ratio typically ranges between 20 and 40 $\text{kg}\,\text{m}^{-2}$ [22]. Taking zero reflectivity, $B = 20\,\text{kg}\,\text{m}^{-2}$ and d equal to the perihelion distance of the asteroid from the Sun yields $a_{\text{SRP}} \approx 2 \times 10^{-7}\,\text{m}\,\text{s}^{-2}$ for both asteroids. In comparison, the centrifugal-induced acceleration acting on the CS, assumed at an altitude of 97 m and 590 m on Bennu and Golevka

respectively, is $5 \times 10^{-5}\,\mathrm{m\,s^{-2}}$ for Bennu and $7 \times 10^{-5}\,\mathrm{m\,s^{-2}}$ for Golevka, about two order of magnitude smaller than a_{SRP}. Therefore it is expected that the solar radiation pressure has a minor effect on the system.

VI. Conclusion

In this paper, the dynamics of an orbital siphon anchored to a non-spherical asteroid has been investigated. The key idea behind the orbital siphon is that a chain of tether-connected masses arranged from the surface of a rotating asteroid can overcome the surface gravity of a rotating body and lift payload masses without the need for external work to be done. By releasing the upper payloads of the chain and adding new payloads at the bottom, an orbital siphon mechanism is initialized and a stream of masses can be delivered from the surface of the body into orbit or to a collecting spacecraft.

Expanding on previous work, here the siphon was modelled as a set of discrete masses connected by tethers and self-supported. Moreover, the material is released to an orbiting collecting spacecraft connected to the siphon which also serves as a counterweight to keep the system in tension. The two near-Earth asteroids 101955 Bennu and 6489 Golevka were selected with the gravitational potential modelled using triangular-faced polyhedron models.

It has been shown that the orbital siphon effect is generated under the model used. This is a key result, as the proposed self-supporting siphon architecture reduces the scale of infrastructure mass with respect to a supported siphon with a truss structure. Moreover, the irregularities of the gravitational potential do not introduce instabilities to the orbital siphon system or irregularly bend the chain in the analysed scenarios. As in previous studies, the chain average velocity does not diverge but reaches a steady state, due to the constant deceleration accompanying each bucket refilling.

The dynamics of a siphon with a moving anchor base has also been considered. It has been shown that the siphon effect is still generated. This would allow the mining location to be moved without interrupting the flow of material to the collecting spacecraft.

Funding Sources

CM is supported by a Royal Academy of Engineering Chair in Engineering Technologies and a Royal Society Wolfson Research Merit Award

References

[1] Sanchez, J., and McInnes, C., "Assessment on the feasibility of future shepherding of asteroid resources," *Acta Astronautica*, Vol. 73, 2012, pp. 49–66. https://doi.org/10.1016/j.actaastro.2011.12.010.

[2] Gerlach, C. L., "Profitably Exploiting Near-Earth Object Resources," *Proceedings of the 2005 International Space Development Conference, National Space Society, Washington DC.*, 2005.

[3] McMahon, J., Mitchell, S. K., Oguri, K., Kellaris, N., Kuettel, D., Keplinger, C., and Bercovici, B., "Area-of-Effect Softbots (AoES) for Asteroid Proximity Operations," *IEEE*, 2019. https://doi.org/10.1109/aero.2019.8741680.

[4] Yárnoz, D. G., Cuartielles, J. P. S., and McInnes, C. R., "Passive Sorting of Asteroid Material Using Solar Radiation Pressure," *Journal of Guidance, Control, and Dynamics*, Vol. 37, No. 4, 2014, pp. 1223–1235. https://doi.org/10.2514/1.62412.

[5] McInnes, C. R., "Dynamics of a Particle Moving Along an Orbital Tower," *Journal of Guidance, Control, and Dynamics*, Vol. 28, No. 2, 2005, pp. 380–382. https://doi.org/10.2514/1.13505.

[6] McInnes, C. R., and Davis, C., "Novel Payload Dynamics on Space Elevator Systems," 2005. https://doi.org/10.2514/6.iac-05-d4.2.07.

[7] Mashayekhi, M., and Misra, A., "Tether assisted near earth object diversion," *Acta Astronautica*, Vol. 75, 2012, pp. 71–77. https://doi.org/10.1016/j.actaastro.2011.12.018.

[8] French, D. B., and Mazzoleni, A. P., "Modeling tether–ballast asteroid diversion systems, including tether mass and elasticity," *Acta Astronautica*, Vol. 103, 2014, pp. 282–306. https://doi.org/10.1016/j.actaastro.2014.04.014.

[9] Zhang, J., Yang, K., and Qi, R., "Dynamics and offset control of tethered space-tug system," *Acta Astronautica*, Vol. 142, 2018, pp. 232–252. https://doi.org/10.1016/j.actaastro.2017.10.020.

[10] Bombardelli, C., "Artificial spin-up and fragmentation of sub-kilometre asteroids," *Acta Astronautica*, Vol. 65, No. 7, 2009, pp. 1162–1167. https://doi.org/10.1016/j.actaastro.2009.03.030.

[11] Kang, J., and Zhu, Z. H., "Dynamics and control of de-spinning giant asteroids by small tethered spacecraft," *Aerospace Science and Technology*, Vol. 94, 2019, p. 105394. https://doi.org/10.1016/j.ast.2019.105394.

[12] Tsiolkovsky, K., *Dreams of the Earth and Sky: Collected Works of Tsiolkovsky*, Amazon Digital Services LLC - Kdp Print Us, 2017.

[13] Artsutanov, Y., "V kosmos na elektrovoze," *Komsomolskaya Pravda*, Vol. 31, 1960, pp. 946–947.

[14] Viale, A., McInnes, C., and Ceriotti, M., "Analytical mechanics of asteroid disassembly using the Orbital Siphon effect," *Proceedings of the Royal Society A: Mathematical, Physical and Engineering Sciences*, Vol. 474, No. 2220, 2018, p. 20180594. https://doi.org/10.1098/rspa.2018.0594.

[15] Viale, A., McInnes, C. R., and Ceriotti, M., "Disassembly of Near Earth Asteroids by Leveraging Rotational Self Energy," *69th International Astronautical Congress, IAC-18-D4.3-18*, 2018. URL http://eprints.gla.ac.uk/168724/.

[16] Werner, R., and Scheeres, D., "Exterior gravitation of a polyhedron derived and compared with harmonic and mascon gravitation representations of asteroid 4769 Castalia," *Celestial Mechanics and Dynamical Astronomy*, Vol. 65, No. 3, 1997. https://doi.org/10.1007/bf00053511.

[17] Nolan, M. C., Magri, C., Howell, E. S., Benner, L. A., Giorgini, J. D., Hergenrother, C. W., Hudson, R. S., Lauretta, D. S., Margot, J.-L., Ostro, S. J., and Scheeres, D. J., "Shape model and surface properties of the OSIRIS-REx target Asteroid (101955) Bennu from radar and lightcurve observations," *Icarus*, Vol. 226, No. 1, 2013, pp. 629–640. https://doi.org/10.1016/j.icarus.2013.05.028.

[18] Chesley, S. R., "Direct Detection of the Yarkovsky Effect by Radar Ranging to Asteroid 6489 Golevka," *Science*, Vol. 302, No. 5651, 2003, pp. 1739–1742. https://doi.org/10.1126/science.1091452.

[19] Scheeres, D., Hesar, S., Tardivel, S., Hirabayashi, M., Farnocchia, D., McMahon, J., Chesley, S., Barnouin, O., Binzel, R., Bottke, W., Daly, M., Emery, J., Hergenrother, C., Lauretta, D., Marshall, J., Michel, P., Nolan, M., and Walsh, K., "The geophysical environment of Bennu," *Icarus*, Vol. 276, 2016, pp. 116–140. https://doi.org/10.1016/j.icarus.2016.04.013.

[20] Chesley, S. R., "Direct Detection of the Yarkovsky Effect by Radar Ranging to Asteroid 6489 Golevka," *Science*, Vol. 302, No. 5651, 2003, pp. 1739–1742. https://doi.org/10.1126/science.1091452, URL https://doi.org/10.1126%2Fscience.1091452.

[21] Mottola, S., Erikson, A., Harris, A. W., Hahn, G., Neukum, G., Buie, M. W., Sears, W. D., Harris, A. W., Tholen, D. J., Whiteley, R. J., Magnusson, P., Piironen, J., Kwiatkowski, T., Borczyk, W., Howell, E. S., Hicks, M. D., Fevig, R., Krugly, Y. N., Velichko, F. P., Chiorny, V. G., Gaftonyuk, N. M., di Martino, M., Pravec, P., Sarounova, L., Wolf, M., Worman, W., Davies, J. K., Schober, H.-J., and Pych, W., "Physical model of near-earth asteroid 6489 golevka (1991 JX) from optical and infrared observations." *The Astronomical Journal*, Vol. 114, 1997, p. 1234. https://doi.org/10.1086/118557.

[22] Scheeres, D. J., *Orbital Motion in Strongly Perturbed Environments*, Springer Berlin Heidelberg, 2012. https://doi.org/10.1007/978-3-642-03256-1.

[23] Gassendy, B., "Non-Equatorial Uniform-Stress Space Elevators," *Proc. 3rd ISEC*, 2004.

[24] Mashayekhi, M. J., Misra, A. K., and Keshmiri, M., "Dynamics of a Tether System Connected to an Irregularly Shaped Celestial Body," *The Journal of the Astronautical Sciences*, Vol. 63, No. 3, 2016, pp. 206–220. https://doi.org/10.1007/s40295-016-0088-y.

[25] Viale, A., McInnes, C. R., and Ceriotti, M., "Dynamics of an orbital siphon anchored to a rotating ellipsoidal asteroid for resource exploitation," *Acta Astronautica, submitted*, 2020.

[26] Zhao, Z., Wang, S., Li, D., Wang, H., Wang, Y., and Zhao, J., "Development of an Anchoring System for the Soft Asteroid Landing Exploration," *International Journal of Aerospace Engineering*, Vol. 2019, 2019, pp. 1–13. https://doi.org/10.1155/2019/1257038.

[27] Cherston, J., Strohmeier, P., and Paradiso, J. A., "Grappler: Array of Bistable Elements For Pinching Net-Like Infrastructure to Low Gravity Bodies," 2019. https://doi.org/10.2514/6.2019-0871.

[28] Hintz, G. R., *Fundamentals of Astrodynamics*, Springer International Publishing, 2015. https://doi.org/10.1007/978-3-319-09444-1_1.